Contactless rheology of finite-size air-water interfaces – Supplementary Material –

Vincent Bertin,[1,2,*] Zaicheng Zhang,[1,*] Rodolphe Boisgard,[1] Christine Grauby-Heywang,[1] Elie Raphaël,[2] Thomas Salez,[1,3,†] and Abdelhamid Maali[1,‡]

[1] *Univ. Bordeaux, CNRS, LOMA, UMR 5798, 33405 Talence, France.*
[2] *UMR CNRS Gulliver 7083, ESPCI Paris, PSL Research University, 75005 Paris, France.*
[3] *Global Station for Soft Matter, Global Institution for Collaborative Research and Education, Hokkaido University, Sapporo, Hokkaido 060-0808, Japan.*

(Dated: June 15, 2021)

I. THEORY

In this model, we neglect gravity and focus on bubbles that are smaller than the capillary length. The bubble's surface profile follows the Young-Laplace equation [1]:

$$\gamma\kappa = \frac{\gamma}{r}\frac{\partial}{\partial r}\left[r\,\frac{\partial h_{\rm b}/\partial r}{\sqrt{1+(\partial h_{\rm b}/\partial r)^2}}\right] = \Delta P(t) + p(r,t)\ , \tag{S1}$$

where κ denotes the bubble surface curvature, which is expressed in cylindrical coordinates (see Fig. (1) in the main article) for an axisymmetric system. The hydrodynamic excess pressure fields is denoted p, and ΔP is the pressure difference across the interface. The Young-Laplace equation can be obtained by minimizing the free energy of the system [2], and the pressure difference ΔP appears as the Lagrange multiplier associated with the volume conservation of the air bubble in this framework. At equilibrium, the pressure difference is $-2\gamma/R_{\rm b}$, where $R_{\rm b}$ is the curvature radius of the bubble and the bubble's surface profile follows a spherical cap. In the following, we write the pressure difference as $\Delta P(t) = -2\gamma/R(t)$, where $R(t)$ is the mean curvature radius in the presence of an excess hydrodynamic pressure field. In addition, we consider acute contact angles θ, as is the case for an air bubble deposited onto a PS substrate within water. Therefore, the bubble's surface profile $h_{\rm b}(r,t)$ is a multivalued function of r, and Eq. (S1) is valid only in the upper part of the bubble, corresponding to the z_+ branch in Fig. S1. One can integrate Eq. (S1) with respect to r and get:

$$\frac{r\partial h_{\rm b}/\partial r}{\sqrt{1+(\partial h_{\rm b}/\partial r)^2}} = -\frac{r^2}{R(t)} + \frac{1}{\gamma}\int_0^r p(r',t)\,r'\,{\rm d}r'\ . \tag{S2}$$

The excess pressure field decays over a typical radial extent $\sim\sqrt{2R_{\rm eff}D}$, that is the usual hydrodynamic radius in lubrication problems, where $R_{\rm eff}$ is the effective curvature radius of the liquid-gap thickness between the sphere and the bubble. We focus on the situations in which this typical hydrodynamic radius is small with respect to the bubble size, yielding the scale separation: $\sqrt{2R_{\rm eff}D} \ll R_{\rm b}$.

A. Outer solution

We use the method of matched asymptotic expansions [3], following specifically Refs. [2, 4]. We first describe the outer solution (denoted with the subscript "out"), which is a good approximation of the solution outside the hydrodynamic region, *i.e.* for $r \gg \sqrt{2R_{\rm eff}D}$. In this limit, the integral $2\pi\int_0^r p(r',t)\,r'\,{\rm d}r'$ does essentially not depend on r and can be approximated by the hydrodynamic force $F(t) = 2\pi\int_0^\infty p(r',t)\,r'\,{\rm d}r'$. Therefore, the outer problem is equivalent to the one schematized in Fig. S1. The solution is derived in Ref. [4], and we recall the main steps here. We drop the time dependencies for conciseness, and the two interfacial branches are denoted $z_\pm$, where + denotes the

*These authors contributed equally.
†Electronic address: thomas.salez@u-bordeaux.fr
‡Electronic address: abdelhamid.maali@u-bordeaux.fr

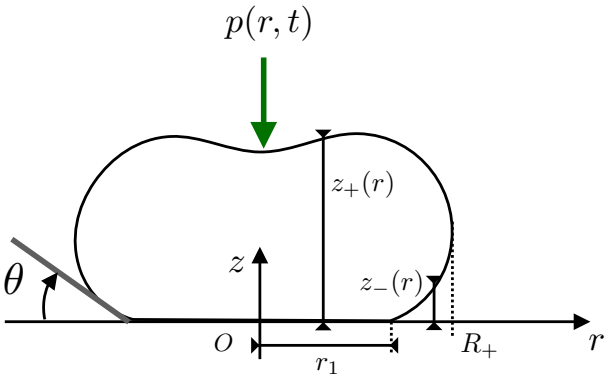

FIG. S1: Schematic of the outer problem.

upper section of the bubble and − the lower section (see Fig. S1). The functions $z_\pm$ are related to the bubble's surface profile via the relation $h_{\rm b,out} = z_\pm - R_{\rm b}(1+\cos\theta)$. Equation (S2) can be written conveniently for both branches as:

$$\pm\frac{r\partial z_\pm/\partial r}{[1+(\partial z_\pm/\partial r)^2]^{1/2}} = -\frac{r^2}{R} + \frac{F}{2\pi\gamma}\,. \tag{S3}$$

The maximal lateral extent R_+ of the bubble (see Fig. S1) can be found by taking the limit $\partial z_\pm/\partial r \to \mp\infty$ in Eq. (S3), and satisfies the polynomial equation:

$$R_+^2/R - R_+ = F/(2\pi\gamma)\,. \tag{S4}$$

Equation (S3) can be integrated and the solution can be expressed using the elliptic integrals of the first and second kinds, $\mathcal{F}$ and $\mathcal{E}$ respectively, and the constant R_+ as:

$$z_\pm(r) = \pm\left[R_+\mathcal{E}(K(r),q) - \frac{F}{2\pi\gamma}\frac{R}{R_+}\mathcal{F}(K(r),q)\right] \mp \left[R_+\mathcal{E}\left(K\left(r_1\right),q\right) - \frac{F}{2\pi\gamma}\frac{R}{R_+}\mathcal{F}\left(K\left(r_1\right),q\right)\right]\,, \tag{S5}$$

with:

$$K(r) = \arcsin\left(\sqrt{\frac{R_+^2-r^2}{R_+^2-(\frac{F}{2\pi\gamma})^2R^2R_+^{-2}}}\right)\,, \qquad q^2 = 1-\frac{(\frac{F}{2\pi\gamma})^2R^2}{R_+^4}\,, \tag{S6}$$

and where r_1 denotes the contact radius of the bubble on the substrate (see Fig. S1) . We focus on situations in which the deviation of the bubble's surface profile is small with respect to the equilibrium spherical cap, *i.e.* in the small-force limit where $\frac{F}{2\pi\gamma} \ll R_{\rm b}$, which allows us to expand Eq. (S5) to leading order in $F/(2\pi\gamma R_{\rm b})$. In this limit, we have $q^2 \approx 1$ and for $r \ll R$, the elliptic integrals can be approximated by $\mathcal{E}(K(r),1) \approx \sin(K(r))$ and $\mathcal{F}\left(K\left(r\right),1\right) \approx \frac{1}{2}\log(\frac{1+\sin(K(r))}{1-\sin(K(r))})$, which yields to an expression for the bubble interface profile near the apex of the bubble:

$$z_+(r) \simeq R\left[1-\frac{r^2}{2R^2}+\sqrt{1-\frac{r_1^2}{R_+^2}}\right] + \frac{F}{2\pi\gamma}\left[1+\sqrt{1-\frac{r_1^2}{R_+^2}}+\frac{1}{2}\log\left(\frac{r^2}{4R^2}\right) - \log\left(\frac{1+\sqrt{1-\frac{r_1^2}{R_+^2}}}{1-\sqrt{1-\frac{r_1^2}{R_+^2}}}\right)\right]\,. \tag{S7}$$

To get an closed expression for the bubble's surface profile near the apex of the bubble, we need to find the relationships between R, R_+ and r_1 and the force F. To do so, we expand the mean curvature radius as:

$$R = R_{\rm b} + \delta R \tag{S8}$$

where δR is a perturbation with respect to the equilibrium value and which scales as $\sim F/(2\pi\gamma)$. Using Eq. (S4), the maximal lateral extend of the bubble is expanded as:

$$R_+ \simeq R_{\rm b} + F/(2\pi\gamma) + \delta R\,. \tag{S9}$$

Here, we assume that the contact line is pinned, which amounts to fix the contact radius to a value $r_1 = R_\mathrm{b}\sin\theta$, where θ is the equilibrium contact angle. The relationship between δR and F can be found expressing the volume conservation of the bubble. The air volume inside the bubble can be evaluated at leading order in $F/(2\pi\gamma R_\mathrm{b})$ using Eq. (S5) and reads:

$$\begin{aligned} V_\mathrm{b} &= 2\pi\int_{r_1}^{R_+} z_-(r)\,r\mathrm{d}r + 2\pi\int_0^{R_+} z_+(r)\,r\mathrm{d}r \\ &\simeq \pi R^3\left[\frac{2}{3}+\frac{1}{3}\sqrt{1-\frac{r_1^2}{R_+^2}}\left(2+\frac{r_1^2}{R^2}\right)+\frac{F}{2\pi\gamma R}\left(1+\sqrt{1-\frac{r_1^2}{R_+^2}}\left(1+\frac{1}{3}\frac{r_1^2}{R^2}\right)\right)\right] . \end{aligned} \tag{S10}$$

Introducing the expansions Eqs. (S8) and (S9) in Eq. (S10), we write the volume variation at leading order as:

$$V_\mathrm{b} - V_{\mathrm{b},0} \simeq \frac{\pi R_\mathrm{b}^2}{\cos\theta}\left[\frac{F}{2\pi\gamma}(1+\cos\theta)+\delta R(1+\cos\theta)^2\right] , \tag{S11}$$

where $V_{\mathrm{b},0} = \pi R_\mathrm{b}^3[2/3+\cos\theta-\cos^3(\theta)/3]$ is the equilibrium bubble volume. Assuming that the bubble is incompressible, we get:

$$\delta R = -\frac{F}{2\pi\gamma}\,\frac{1}{1+\cos\theta} . \tag{S12}$$

Therefore, the bubble's surface profile near the apex of the bubble in Eq. (S7), reads:

$$z_+(r) \simeq R_\mathrm{b}\left(1+\cos\theta-\frac{r^2}{2R_\mathrm{b}^2}\right)+\frac{F}{2\pi\gamma}\left[1+\log\left(\frac{r}{2R_\mathrm{b}}\right)-\log\left(\frac{1+\cos\theta}{1-\cos\theta}\right)\right], \tag{S13}$$

and, thus, the outer solution finally reads for $r \ll R_\mathrm{b}$:

$$h_{\mathrm{b,out}} \simeq -\frac{r^2}{2R_\mathrm{b}}+\frac{F}{2\pi\gamma}\left[1+\log\left(\frac{r}{2R_\mathrm{b}}\right)-\log\left(\frac{1+\cos\theta}{1-\cos\theta}\right)\right] . \tag{S14}$$

B. Inner solution

We now focus on the inner asymptotic solution (denoted with the subscript "in"), in the region near the apex of the bubble, for which the radial coordinate r of the same order as the hydrodynamic radius $\sqrt{2R_\mathrm{eff}D}$. In this region, the slope $\partial_r h_{\mathrm{b,in}}$ of the bubble's surface profile is small with respect to unity, such that Eq. (S1) can be linearized into:

$$\frac{\gamma}{r}\frac{\partial}{\partial r}\left(r\,\frac{\partial h_{\mathrm{b,in}}}{\partial r}\right) = \Delta P(t) + p(r,t) . \tag{S15}$$

Therefore, we can expand the bubble's surface profile as the sum of a parabolic equilibrium shape and a deviation $u_\mathrm{in}(r,t)$, *i.e.* : $h_{\mathrm{b,in}}(r,t) \simeq -\frac{r^2}{2R_\mathrm{b}} - u_\mathrm{in}(r,t)$. Using the expansion of the pressure difference $\Delta P(t) = -\frac{2\gamma}{R} \simeq -2\gamma/R_\mathrm{b} + 2\gamma\delta R(t)/R_\mathrm{b}^2$, with Eq. (S12) and the linear properties of Eq. (S15), we find:

$$-\frac{\gamma}{r}\frac{\partial}{\partial r}\left(r\,\frac{\partial u_\mathrm{in}}{\partial r}\right) = -\frac{F(t)}{\pi R_\mathrm{b}^2}\frac{1}{1+\cos\theta} + p(r,t) . \tag{S16}$$

The inner solution must match asymptotically the outer solution of Eq. (S14), which imposes the following asymptotic expression at $r \gg \sqrt{2R_\mathrm{eff}D}$:

$$u_\mathrm{in} \sim -\frac{F(t)}{2\pi\gamma}\left[1-\log\left(\frac{1+\cos\theta}{1-\cos\theta}\right)+\log\left(\frac{r}{2R_\mathrm{b}}\right)\right] . \tag{S17}$$

Finally, in order to write the problem in a closed form, we need to solve the hydrodynamic equation. The excess pressure field follows the Reynolds equation:

$$\frac{\partial h(r,t)}{\partial t} = \frac{1}{12\eta r}\frac{\partial}{\partial r}\left[r h(r,t)^3\frac{\partial}{\partial r}p(r,t)\right] , \tag{S18}$$

where $h(r,t) = D + Z(t) + \frac{r^2}{2R_\mathrm{s}} - h_\mathrm{b}(r,t)$ is the liquid gap thickness. The sphere's surface profile is written here with the parabolic assumption. Combining the latter with the above expansion for $h_{\mathrm{b,in}}(r,t)$, we find:

$$h(r,t) = D + \frac{r^2}{2R_\mathrm{eff}} + Z(t) + u_\mathrm{in}(r,t) \ . \tag{S19}$$

The modulus $|Z^*|$ of the amplitude Z^* of the vertical displacement Z of the sphere and the deformation of the bubble are assumed to be much smaller than the average sphere-bubble distance D, so that we can neglect the contributions of Z and u_in in the non-linear ($\propto h^3$) factor within the Reynolds equation. The complex version of the latter thus becomes at leading order:

$$12\eta r i\omega \left[Z^* + u^*_\mathrm{in}(r) \right] = \frac{\mathrm{d}}{\mathrm{d}r}\left[r \left(D + \frac{r^2}{2R_\mathrm{eff}} \right)^3 \frac{\mathrm{d}p^*(r)}{\mathrm{d}r} \right] . \tag{S20}$$

Similarly, Eq. (S16) written with complex variables reads:

$$-\frac{\gamma}{r}\frac{\mathrm{d}}{\mathrm{d}r}\left(r \frac{\mathrm{d}u^*_\mathrm{in}}{\mathrm{d}r} \right) = \frac{G^* Z^*}{\pi R_\mathrm{b}^2} \frac{1}{1+\cos\theta} + p^*(r) \ . \tag{S21}$$

Finally, we introduce the dimensionless variables:

$$x = \frac{r}{\sqrt{2R_\mathrm{eff} D}} \ , \qquad U^*_\mathrm{in} = \frac{u^*_\mathrm{in}}{Z^*} \ , \qquad P^* = \frac{p^*}{\frac{\eta R_\mathrm{eff} Z^* \omega}{D^2}} \ , \qquad \mathcal{G}^* = \frac{G^* D_\mathrm{c}}{6\pi\eta\omega R_\mathrm{eff}^2} \ , \qquad D_\mathrm{c} = \frac{16 R_\mathrm{eff}^2 \eta\omega}{\gamma} \ , \tag{S22}$$

such that Eqs. (S20) and (S21) become:

$$24 i \left[1 + U^*_\mathrm{in}(x) \right] = \frac{1}{x}\frac{\mathrm{d}}{\mathrm{d}x}\left[x \left(1+x^2\right)^3 \frac{\mathrm{d}P^*(x)}{\mathrm{d}x} \right] , \tag{S23}$$

$$-\frac{1}{x}\frac{\mathrm{d}}{\mathrm{d}x}\left(x \frac{\mathrm{d}U^*_\mathrm{in}}{\mathrm{d}x} \right) = \frac{2R_\mathrm{eff} D}{R_\mathrm{b}^2} \frac{3}{16} \frac{1}{1+\cos\theta} \mathcal{G}^* + \frac{D_\mathrm{c}}{8D} P^*(x). \tag{S24}$$

Then, Eqs. (S23) and (S24) are solved numerically using a standard finite-difference scheme. The boundary conditions are set to:

$$\frac{\mathrm{d}P^*}{\mathrm{d}x}(0) = 0 \ , \qquad P^*(x_\mathrm{max}) = 0 \ , \tag{S25}$$

and:

$$U^*_\mathrm{in}(x_\mathrm{max}) = \frac{3}{8}\mathcal{G}^* \left[1 - \log\left(\frac{1+\cos\theta}{1-\cos\theta} \right) + \log\left(\frac{r_\mathrm{max}}{2R_\mathrm{b}} \right) \right] \ , \tag{S26}$$

where $x_\mathrm{max} = r_\mathrm{max}/\sqrt{2R_\mathrm{eff} D}$ and r_max are the dimensionless boundary and corresponding real boundary of the numerical domain, respectively. The boundary condition Eq. (S26) is set following the asymptotic expression Eq. (S17), which means that r_max is a typical radius that matches the two asymptotic solutions. We checked that the solution is not dependent on r_max, provided that $\sqrt{2R_\mathrm{eff} D} \ll r_\mathrm{max} \ll R_\mathrm{b}$. We notice that another possible method is to use the Hankel transform framework, following Ref. [5] for elastohydrodynamic couplings. For an elastic kernel, the set of equations is reduced into a single Fredholm integral equation for the pressure field in Hankel space, which is then inverted numerically. Here, due to the finite size, the Hankel transform is not appropriate but the Fourier-Bessel series can be employed instead, leading to an infinite series for the pressure field. We have verified that this additional method and our numerical finite-difference method lead to the same mechanical impedance.

C. Large-distance asymptotic model

In this section, we perform an asymptotic calculation at large distance in the inner model. We assume that D_c/D is a small parameter, and we perform the following first-order expansions:

$$U^*_\mathrm{in}(x) \simeq 0 + \frac{D_\mathrm{c}}{D} U^*_{\mathrm{in},1}(x) \ , \tag{S27}$$

$$P^*(x) \simeq P_0^*(x) + \frac{D_\mathrm{c}}{D} P_1^*(x) \ , \tag{S28}$$

$$\mathcal{G}^* \simeq \mathcal{G}_0^* + \frac{D_\mathrm{c}}{D} \mathcal{G}_1^* \ . \tag{S29}$$

The leading-order term P_0^* is given by Eq. (S23) in the undeformed-bubble limit, and reads:

$$P_0^*(x) = -\frac{3i}{(1+x^2)^2} \ , \tag{S30}$$

which gives to the classical Reynolds force:

$$\mathcal{G}_0^*(x) = i\frac{D_c}{D} \ . \tag{S31}$$

Then, the leading-order term $U_{\mathrm{in},1}^*$ is found by inserting P_0^* in Eq. (S24), and by invoking the boundary condition of Eq. (S26). We find:

$$\begin{aligned} U_{\mathrm{in},1}^*(x) = \frac{2R_\mathrm{eff}D}{R_\mathrm{b}^2} \frac{3i}{32} \left(x_\mathrm{max}^2 - x^2\right) \frac{1}{1+\cos\theta} - \frac{3i}{32} \left[\log\left(1+x_\mathrm{max}^2\right) - \log\left(1+x^2\right)\right] \\ + \frac{3i}{16} \left[1 - \log\left(\frac{1+\cos\theta}{1-\cos\theta}\right) + \log\left(\frac{r_\mathrm{max}}{2R_\mathrm{b}}\right)\right] \ . \end{aligned} \tag{S32}$$

In what follows, we neglect the first term of the right-hand side of Eq. (S32) to keep the leading order in $r_\mathrm{max}/R_\mathrm{b}$. Then, introducing $U_{\mathrm{in},1}^*$ in Eq. (S23) allows us to express the next-order correction in pressure:

$$\begin{aligned} P_1^*(x) = \frac{3}{32} \Bigg[\frac{-3 - 6\log\left(\frac{1+\cos\theta}{1-\cos\theta}\right) - 6x^2 + 6\log(\frac{r_\mathrm{max}}{R_\mathrm{b}}) - 3\log 4 - 3\log\left(1+x_\mathrm{max}^2\right)}{(1+x^2)^2} + \pi^2 \\ - 6\frac{\log(1+x^2)}{1+x^2} + 3\log^2(1+x^2) + 6\mathrm{Li}_2(-x^2) \Bigg] \ , \end{aligned} \tag{S33}$$

where Li_2 denotes the dilogarithm function [6]. After some algebra, we find that:

$$\mathcal{G}_1^* = \frac{3}{32} \left(\frac{D_\mathrm{c}}{D}\right) \left[-3 + \log(4) - 2\log\left(\frac{1+\cos\theta}{1-\cos\theta}\right) - 2\log\left(\frac{r_\mathrm{max}}{R_\mathrm{b}}\right) + \log\left(1+x_\mathrm{max}^2\right) \right] . \tag{S34}$$

Finally, assuming that the boundary coordinate x_max is much larger than unity, we get:

$$\mathcal{G}_1^* \simeq \frac{3}{32} \left(\frac{D_\mathrm{c}}{D}\right) \left[-3 + \log(4) - 2\log\left(\frac{1+\cos\theta}{1-\cos\theta}\right) + \log\left(\frac{R_\mathrm{b}^2}{2R_\mathrm{eff}D}\right) \right] , \tag{S35}$$

which is the dimensionless equivalent of Eq. (6) in the main text.

II. EXPERIMENTS

A. Gap-distance determination

The bubble is deposited on a rigid substrate and is approached towards the spherical colloidal probe by imposing an external vertical displacement of the substrate, using a piezo device with a low velocity. Therefore, the position of the bubble's tip, at rest, is known up to a piezo offset (conveniently incorporating the bubble size too). Besides, the hydrodynamic interaction on the spherical probe is triggered by the faster imposed base oscillation of the cantilever. Importantly, the time-averaged hydrodynamic interaction is zero, implying that the DC component of the cantilever's deflection is zero (see Fig. S2). Therefore, the average position of the spherical probe's tip is known, up to another piezo offset (conveniently incorporating the probe and cantilever sizes too). Since the time-averaged vertical deformation of the bubble induced by the hydrodynamic pressure is also zero, the average gap distance D is eventually obtained, up to a combined offset, by subtracting the average probe and bubble's tip positions. Finally, the actual $D = 0$ contact position is determined as the point where the deflection increases sharply from zero (see Fig. S2), thus removing any offset at the end.

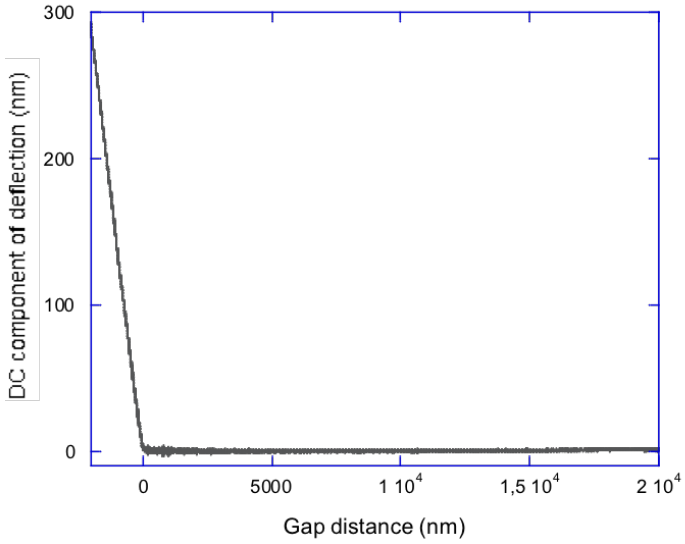

FIG. S2: Raw AFM data of the DC component of the cantilever's deflection vs average gap distance D.

B. Raw amplitude and phase data

The experimental raw data for the results presented in Fig. 2a of the main article is shown in Fig. S3. Figure S3(a) shows the amplitude and phase $(A_\infty, \varphi_\infty)$ versus the oscillation frequency measured far from the surface ($D = 400\ \mu$m), where the interaction can be neglected. Figure S3(b) shows the measured amplitude A and phase φ of the cantilever oscillation versus the separation distance D, for the experiments performed on: i) a reference polystyrene (PS) surface, and ii) a bubble. Indeed, the base amplitude is a priori unknown. We have thus performed a preliminary calibration experiment, with a PS layer spin-coated onto a silica glass. The PS is hard enough to avoid any measurable deformation. In this rigid situation, the storage impedance vanishes ($G' = 0$), and at the PS surface the loss impedance diverges ($G'' = 6\pi\eta R^2\omega/D \to \infty$). This implies that near the PS surface (green line in Fig. (S3b)), the amplitude of the cantilever's deflection is nearly equal to the base amplitude ($A = A_\mathrm{b}$). In practice, the amplitude of the base oscillation was determined as the measured amplitude just before contact with the PS surface (see inset of Fig. (S3b)). Using Eq. (2) of the main article, with the values measured above, one could calculate the mechanical impedance $G^* = -F^*/Z^*$ for each distance D.

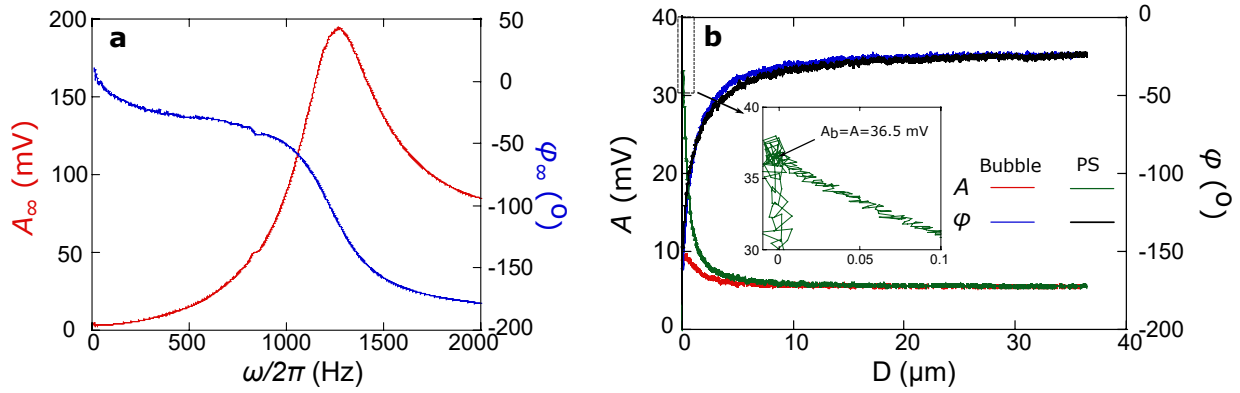

FIG. S3: a) Amplitude A_∞ and phase φ_∞ versus oscillation frequency $\omega/(2\pi)$, measured at a distance $D = 400\ \mu$m. b) Amplitude A and phase φ of the cantilever's oscillation versus D, for the experiments with: i) a PS surface, and ii) a bubble. The frequency is $\omega/(2\pi) = 200$ Hz.

C. AFM resonances

We have employed a liquid cell (DTFML-DDHE, Bruker) that allows for a direct excitation of the cantilever. The cantilever's excitation spectrum shown in Fig. S3(a) is clean and free from spurious peaks related to the mechanical resonances of the AFM.

[1] P.-G. De Gennes, F. Brochard-Wyart, and D. Quéré, Capillarity and wetting phenomena: drops, bubbles, pearls, waves (Springer Science & Business Media, 2013).
[2] D. Y. Chan, E. Klaseboer, and R. Manica, Soft Matter **7**, 2235 (2011).
[3] E. J. Hinch, Perturbation Methods, Cambridge Texts in Applied Mathematics (Cambridge University Press, 1991).
[4] D. Bardos, Surface science **517**, 157 (2002).
[5] S. Leroy and E. Charlaix, Journal of Fluid Mechanics **674**, 389 (2011).
[6] M. Abramowitz and I. A. Stegun, Handbook of mathematical functions with formulas, graphs, and mathematical tables, vol. 55 (US Government printing office, 1948).